

Title: Segmentation of the C57BL/6J mouse cerebellum in magnetic resonance images

Author names:

Jeremy F.P. Ullmann^{b,*,#}, Marianne D. Keller^{b,#}, Charles Watson^{a,c,#}, Andrew L. Janke^b, Nyoman D. Kurniawan^b, Zhengyi Yang^b, Kay Richards^d, George Paxinos^{a,e}, Gary F. Egan^{a,f,g}, Steven Petrou^{a,d}, Perry Bartlett^{a,h}, Graham J. Galloway^{a,b}, David C. Reutens^{a,b}

Affiliations:

^a The Australian Mouse Brain Mapping Consortium, The University of Queensland, Brisbane, Australia.

^b Centre for Advanced Imaging, The University of Queensland, Brisbane, Australia.

^c Health Sciences, Curtin University, Bentley, Western Australia, Australia

^d Florey Neuroscience Institutes, Parkville, Victoria, Australia.

^e Neuroscience Research Australia, The University of New South Wales, Sydney, New South Wales, Australia.

^f Monash Biomedical Imaging, Monash University, Clayton, Victoria, Australia.

^g School of Psychology & Psychiatry, Monash University, Clayton, Victoria, Australia.

^h Queensland Brain Institute, The University of Queensland, Brisbane, Australia.

* Indicates corresponding author

Contributed equally to this work

Contact details:

Dr Jeremy F.P. Ullmann
Centre for Advanced Imaging (Bldg 60)
The University of Queensland
Brisbane, QLD 4072
Australia

E: j.ullmann@uq.edu.au

T: +617 3346 9963

F: +617 3365 3833

Highlights:

- We present a methodology for systematic delineation of the C57BL/6J mouse cerebellum in MRI.
- We have successfully delineated 38 cerebellar and cerebellar-related structures.
- We have calculated average region volumes and created probabilistic maps for each structure.

Keywords:

cerebellum, vermis, magnetic resonance, probabilistic map, mouse brain, atlas, segmentation

Abbreviations:

Magnetic resonance imaging, MRI; Primary fissure, prf; Preculminate fissure, pcuf; Precentral fissure, pcn; Superior fissure, psf; Prepyramidal fissure, ppf; Secondary fissure, sf; Posterolateral fissure, plf; Intercrural fissure, icf; Ansoparamedian fissure,

apmf; Lobule 1, 1Cb; Lobule 2, 2Cb; Lobule 3, 3Cb; Lobules 4/5, 4/5Cb; Lobule 6, 6Cb; Lobule 7, 7Cb; Lobule 8, 8Cb; Lobule 9, 9Cb; Lobule 10, 10Cb; Simple lobule, Sim; Crus 1 of the ansiform lobule, Crus 1; Crus 2 of the ansiform lobule, Crus 2; Paramedian lobule, PM; Copula of the pyramis, Cop; Paraflocculus, PFI; Flocculus, Fl; Lateral cerebellar nucleus, Lat; Lateral cerebellar nucleus, parvicellular part, LatPC; Medial cerebellar nucleus, Med; Medial cerebellar nucleus, lateral part, MedL; Medial cerebellar nucleus, dorsolateral protuberance, MedDL; Interposed cerebellar nucleus, anterior, IntA; Interposed cerebellar nucleus, posterior, IntP; Interposed cerebellar nucleus, posterior parvicellular part, IntPPC; Interposed cerebellar nucleus, dorsolateral hump, IntDL; Dorsal cochlear nuclei, DC; Ventral cochlear nuclei, anterior part, VCA; Ventral cochlear nuclei, posterior part, VCP; Superior cerebellar peduncle, scp; Decussation of the superior cerebellar peduncle, xscp; Middle cerebellar peduncle, mcp; Inferior cerebellar peduncle, icp; Dorsal acoustic stria, das; Superior medullary velum, SMV; Ventral spinocerebellar tract, vsc.

Abstract

The C57BL mouse is the centrepiece of efforts to use gene-targeting technology to understand cerebellar pathology, thus creating a need for a detailed magnetic resonance imaging (MRI) atlas of the cerebellum of this strain. In this study we present a methodology for systematic delineation of the vermal and hemispheric lobules of the C57BL/6J mouse cerebellum in magnetic resonance images. We have successfully delineated 38 cerebellar and cerebellar-related structures. The higher signal-to-noise ratio achieved by group averaging facilitated the identification of anatomical structures. In addition, we have calculated average region volumes and created probabilistic maps for each structure. The segmentation method and the probabilistic maps we have created will provide a foundation for future studies of cerebellar disorders using transgenic mouse models.

1. Introduction

The cerebellum is involved in motor control and motor learning, especially in the coordination of body position, limb movement, and visual input (Glickstein, 2007). Cerebellar lesions in humans result in a wide variety of syndromes, generally characterized by nystagmus, intention tremor, and appendicular and truncal ataxia (Donaghy, 2009). The mouse cerebellum has become the model of choice for investigation of cerebellar disorders because of the availability of relevant mouse mutants and, more recently, the availability of gene targeting technology (Sillitoe et al., 2012). In particular, the C57BL mouse has become the focus of attempts to study the role of genes in the development and function of the cerebellum. This approach has been further facilitated by the website presenting the expression of over 20,000 genes in the mouse brain developed by Allen Brain Institute.

The anatomy of the C57BL mouse cerebellum is well characterized and several histology-based atlases have used cytoarchitectonic and chemoarchitectonic features to establish structural delineations in individual brains (Dong, 2008; Franklin and Paxinos, 2008; Hof et al., 2000; Watson and Paxinos, 2010). Histological atlases are typically based on a single specimen and therefore do not capture the anatomical variability in the cerebellum. In contrast, MRI permits the registration of multiple data sets and has the potential to assess anatomical variability (Dorr et al., 2008; Kovacevic et al., 2005; Ma et al., 2005). However, existing MRI-based atlases have typically identified five or fewer segmented cerebellar structures, limiting the level at which statistical and computational comparisons between individuals or groups can be performed. MRI also permits the examination of the cerebellar anatomy *in vivo*, thereby facilitating examination of longitudinal changes in cerebellar structure over time.

In this paper we present a detailed protocol for segmenting the cerebellum on high-resolution MRI, and we offer an atlas of the *ex vivo* cerebellum of the C57BL/6J mouse. In addition, we applied the segmentation to a model created from 18 brains and assessed the normal variability in the anatomical structures of the C57BL/6J cerebellum.

2. Materials and methods

2.1 C57BL/6J mouse brain preparation and magnetic resonance imaging

Eighteen animals (male, 12 week old) were perfused and fixed with 4% paraformaldehyde and 0.1% Magnevist® (gadopentetate dimeglumine, Bayer HealthCare Pharmaceuticals Inc., Wayne, NJ, USA) in phosphate buffer (PB). Brains were extracted and incubated in 0.1% Magnevist/PB for 4 days, placed in Fomblin (Solvay Solexis, Milan, Italy) and imaged on a 16.4T (89mm) Bruker micro-imaging system (Bruker Biospin, Karlsruhe, Germany) using a 15 mm SAW coil (M2M Imaging, USA). MRI data were acquired using a 3D gradient echo sequence with a repetition time = 50ms, echo time = 12ms, flip angle = 30°, 82 KHz spectral bandwidth, FOV = 2.1 x 1.5 x 0.75 cm, matrix = 700 x 350 x 250, 8 averages, resulting in a total acquisition time of 5h 15mins, to produce T₁/T₂*-weighted images at 30µm isotropic resolution.

2.2 Model creation

Images were placed in the Waxholm stereotaxic coordinate space (Johnson et al., 2010) and a symmetric model was created using a recursive non-linear hierarchical fitting strategy similar to that employed by Fonov et al. (2011) The final fitting step used a nonlinear transformation with a step size of 30µm. Interpolation resulted in a model with 15 µm³ isotropic voxels.

2.3 Segmentation

The major anatomical features of the cerebellum were primarily identified on the coronal slices of the model by a single expert anatomist (CW). Anatomical features were mapped on the basis of differences in signal intensity and/or their location in reference to cerebellar fissures, with constant reference to the histological atlas of Franklin and Paxinos (2008). Structures were then partitioned using vector-based segmentation via a Cintiq tablet (Wacom Company, Ltd). The complete data set was then exported to Amira (Visage Imaging, Inc.) where structural boundaries were checked in the other two orthogonal planes by JFPU and CW. The nomenclature and abbreviations used here were taken from Franklin and Paxinos (2008) and the color palette for cerebellar structures is based on that use in the BrainNavigator (Elsevier Inc.) system. Finally, smoothed three-dimensional surface reconstructions were created in Amira.

2.4. Construction of probabilistic maps

A probabilistic model was created using the same method as that was previously employed to create the average ICBM152 model of the human brain (Collins et al., 1995). The segmented structures from the average model were nonlinearly transformed back to native space and a lower order nonlinear native space to model space transform was then applied. In our case this was a grid transform with a step size of four times the voxel size of the model (60µm). We then assessed the probability of a particular voxel in Waxholm space being occupied by the structure of interest using the number of brains from the 18 datasets in which this was the case. A probability of 1 (100%) for a given voxel signifies that all individual segmentations in the 18 brains overlap at that voxel.

3. Results

The cerebellum was segmented into major regions and sub-regions and the average volume for each structure was computed (Table 1). While the boundaries of major cerebellar regions and subregions were originally defined on the basis of histological features and histology-based mouse brain atlases served as the foundation for defining the borders, the level of contrast and resolution achieved in the model permitted identification of the majority of cerebellar structures without the need for direct histological confirmation in our set of brains.

3.1 Identification of anatomical boundaries

We have segmented the cerebellum according to the scheme originally developed by (Bolk, 1906), and subsequently refined and expanded by (Larsell, 1952, 1970). The Bolk/Larsell scheme has since been adopted by all major modern atlases of the mouse brain (Dong, 2008; Franklin and Paxinos, 2008; Sidman et al., 1971; Watson and Paxinos, 2010). The mouse cerebellum consists of a central vermis and two lateral hemispheres. The vermis is delineated, at least in part, from the hemispheres by paramedian sulci. The vermis consists of a series of ten lobules (1Cb to 10Cb) separated by a series of named fissures. Each of the ten lobules has a traditional name which was current before the development of the Bolk/Larsell scheme: lobule 1 is the lingula; lobules 2 and 3 are the central lobule; lobules 4 and 5 are the culmen; lobule 6 is the declive; lobule 7 is the folium and tuber; lobule 8 is the pyramis; lobule 9 is the uvula; and lobule 10 is the nodulus. In the mouse, the anterior lobe vermal lobules (lobules 1 to 5) do not contribute to the cerebellar hemispheres, but each of lobules 6 to 10 has a substantial extension into the hemisphere: lobule 6 extends into the simple lobule and crus 1 of the ansiform lobule; lobule 7 extends into crus 2 of the ansiform lobule and the paramedian lobule; lobule 8 extends into the copula of the pyramis; lobule 9 extends into the flocculonodular lobe; and lobule 10 extends into the flocculus. While lobules 6-8 can be seen to be directly continuous with their lateral extensions, lobules 9 and 10 are more difficult to visualize. The reason is that the flocculus and paraflocculus are displaced rostrally with an attenuated connection to their parent lobules.

3.2 Fissures

The key to cerebellar segmentation is the identification of the fissures. The fissures separate the major vermal lobules and the parts of the cerebellar hemispheres (Fig. 1). When attempting to identify the fissures it is useful to refer to a mid-sagittal section of cerebellum (Fig. 1a). Note that a fissure separating two lobules must have a molecular layer on each side, while the mid-space between any two fissures should be a strip of white matter.

The primary fissure (prf) extends coronally between lobules 5 and 6 to separate the vermis into rostral and caudal lobes. Located in the anterior lobe and positioned rostral to the primary fissure is the preculminate fissure (pcuf), which separates lobules 4 and 3, and the precentral fissure (pcn), which separates lobules 3 and 2. Caudal to the primary fissure is the posterior superior fissure (psf), which is a shallow fissure that separates lobule 6 and 7, the prepyramidal fissure (ppf), which separates lobules 7 and 8, and the secondary fissure (sf), which is a deep fissure found between lobule 8 and 9. Finally, the posterolateral fissure (plf) separates lobule 10 (the nodule) from lobule 9.

Two fissures, psf and, ppf extend the entire width of the cerebellum to subdivide also the cerebellar hemispheres. The psf creates a boundary between the simple lobule and crus 1 of the ansiform lobule whilst the ppf separates the copula from the paramedian lobule. In addition, the intercrural fissure (icf) divides the ansiform lobule into the rostral crus 1 and the caudal crus 2 and the ansoparamedian fissure (apmf) separates the paramedian lobule from crus 2 of the ansiform lobule.

3.3 Segmentation of the vermis and hemispheres

A detailed segmentation guide for each of the 38 structures is available in the supplementary data section. We provide an example here:

The most rostral parts of the cerebellum first appear lateral to the two inferior colliculi (IC) and then between the colliculi. Lateral to each colliculus is the lateral extension of the combined lobule 4/5 (4/5Cb), and just below is the flocculus (Fl) (Fig. 2A, B). Between the two colliculi the first part of the vermis to appear is lobule 2 (2Cb), closely followed by lobule 3 (3Cb). Both of these are nested in the space between colliculi. The central (vermal) part of lobule 4/5 (4/5Cb) appears dorsal to the colliculi (Fig. 2C, D). At this level the lateral extension of 4/5Cb is joined dorsolaterally by the simple lobule (Sim) and the rostral part of crus 1 of the ansiform lobule (Crus 1).

3.4 Probabilistic maps

The probabilistic map for all structures within the cerebellum is shown in the supplementary data section, Fig. 1. The locations of the images are given in Waxholm space. The maps demonstrate inter-specimen anatomical variability observed in the PM (y = 7.9 and 5.7), PFl (y=6.5), 10Cb (y = 5.7), and VCP (y= 6.3). Additional variability is also observed along borders, fissures and sulci including the border between 4/5Cb and the Crus 1 (y = 6.3) and 9Cb and 10Cb (y = 7.3). Differences can also be observed between the left and right vermis, as seen in the left PFL, which does not match the symmetric model, as well as the right PRL (y = 5.7, 5.9).

3.5 Three-dimensional reconstructions

Three-dimensional surface reconstructions of the cerebellum and associated structures are shown in Fig. 5 and in Supplementary videos 1 and 2.

4. Discussion

In creating this MRI-based C57BL/6J mouse cerebellum atlas we have defined 38 cerebellar and cerebellar-related structures, including vermal and hemispheric lobules, and cerebellar, vestibular, and cochlear nuclei. This is a significant improvement over other MRI-based atlases, including: Ma et al. (2005) who did not subdivide the cerebellum, Dorr et al. (2008) who divided the cerebellum into five regions, and Johnson et al. (2010) who did not subdivide the cerebellum.

The anatomy of the C57BL/6J cerebellum has been described in a recent book chapter (Sillitoe et al., 2012). This review presents the gross anatomy, lobular organization, and histology of the cerebellum, and the authors summarize the distinctive features of the C57BL/6J cerebellum compared to that of other mouse strains. For example, when compared with the DBA/2T mouse, the C57BL/6J lacks an interculminate fissure, which results in incomplete separation of lobules 4 and 5, and, in addition, the

boundary between lobules 1 and 2 is difficult to define (Neumann et al., 1993; Neumann et al., 1990).

The proposed protocol for the segmentation of the cerebellum aims to support a consistent approach to quantitative studies of regional volumes in the cerebellum. Our approach is primarily based upon the identification of cerebellar fissures as the fissures separate the major vermal lobules and the parts of the cerebellar hemispheres. One of the challenges we faced in segmenting the cerebellum is that there is often no clear anatomical boundary (e.g. fissure) between vermal and hemispheric regions in the C57BL/6J cerebellum and therefore no clear boundary on the MRIs. For example, there is no fissure between lobule 8 and crus 2 of the ansiform lobule and very little contrast difference with average signal intensity values as a percent of the maximum of 75.2 and 74.6 respectively (see Fig. 3C, D). We thus developed a reproducible geometric method of separating the vermis and hemisphere where a clear sulcus is not visible.

In contrast to other research groups, which utilized *in vivo* imaging to create their atlases (Ma et al., 2008; Quallo et al., 2010) we specifically chose *ex vivo* imaging as it eliminated motion artifacts and enabled small fields of view and long scan times. Although some damage could have occurred during dissection, we did not observe any major deformations on visual inspection. It should be noted that our *ex vivo* images have not undergone the sectioning and histological processing undergone by brains used in the current ‘gold-standard’ histological atlases and which may induce significant deformations in the latter. Moreover, to create a detailed atlas of the mouse cerebellum we required the high spatial resolution ($15\ \mu\text{m}^3$) obtained with *ex vivo* imaging and the increased signal to noise ratio achieved through group averaging. As seen in Fig. 6b, a lower resolution ($100\ \mu\text{m}$) permits the identification of the major cerebellar regions but not precise identification of the majority of structural boundaries and visualization of cerebellar nuclei. Therefore, we advise those engaged in cerebellar research to consider the aim of their research project before proceeding with high-resolution imaging. It is possible that a less expensive and quicker scan could be adequate for some purposes.

4.2 C57BL/6J cerebellum

Inouye and Oda (1980) have documented the inter-strain variation that exists in the mouse cerebellum and have shown that each inbred strain possesses a distinctive folial pattern (Inouye and Oda, 1980). In this study we attempted to determine the range of intra-strain variation in the C57BL/6J cerebellum. We found that the location of each of the vermal and hemispheric lobules is relatively constant. The location of lobules 3, 7, and 8, the simple lobule, and crus 2 all have probability values of 1.0. In contrast, the paraflocculus, which had a value of approximately 0.5, the caudal edge of the paramedian lobule, which had a value of approximately 0.15, and lobule 1, which had a value between 0.5 - 0.75, showed higher variability. However, the observed variability of these structures may be due to less marked MRI signal intensity change between structures in the caudal end of the cerebellum, in addition to the natural variability between specimens. The variability found in the paraflocculus and paramedian lobule could also result from damage to these small border structures during preparation of the brain for *ex vivo* imaging.

Brains used in this study were fixed with a solution containing a contrast agent. This increases tissue contrast and may affect the registration of non-contrast specimens to the brain model and hence the atlas. The impact of differences in contrast on registration error requires assessment before the atlas is employed for automated segmentation of the cerebellum prepared or imaged using other techniques. Our segmentation protocol is based primarily upon the identification of the cerebellar fissures. Imaging sequences and techniques that enable the visualization of these structures would be a pre-requisite for accurate automated segmentation. The creation of MDA probabilistic maps always includes some error as a result of the difficulties associated with the image registration process. Structures with well-defined boundaries will generally align more consistently to an average that exhibits these same structures. This will in turn result in a lower variance associated with these structures. An image boundary in the centre of a larger structure will improve the registration, as there will be a smaller area over which the algorithm has to interpolate deformation results. Notwithstanding this, significant morphometric variance in a population will overshadow the effect of registration bias. This is particularly true for the cerebellum, which develops post-natally in response to sensory feedback.

Conclusion




































The probabilistic mouse cerebellum atlas generated in this study can be used as a template for research on transgenic strains of mice that are used as models for human cerebellar disease. It provides a detailed and comprehensive classification of the canonical C57BL/6J mouse cerebellum with operational criteria defining anatomical boundaries as well as normative structural volumes and probabilistic maps. The atlas will assist the segmentation of the cerebellum of novel mutants with C57BL/6J backgrounds and will permit the identification of altered morphologies. This atlas is a significant addition to the existing atlases. The atlas, probabilistic atlases of individual structures and three dimensional surface reconstructions are available for download at the Australian Mouse Brain Mapping Consortium (AMBMC) website: <http://www.imaging.org.au/AMBMC>.

Acknowledgments

We would like to thank the National Imaging Facility (NIF) and the Queensland NMR Network (QNN) for access to the 16.4T scanner and technical support. This project was funded by the National Health and Medical Research Council (NHMRC) of Australia.

Table 1

Cerebellum segmentation in coronal sections using T_2^* -weighted images. For each region, there is an abbreviation, color code for the figures, an average volume measurement, and its average signal intensity as a percent of the maximum.

Structure	Abbreviation	Color Code	Average Volume (mm ³)	Average Signal Intensity (%)
<i>Lobules of cerebellar vermis</i>				
Lobule 1	1Cb		0.14	83.5
Lobule 2	2Cb		1.16	84.3
Lobule 3	3Cb		1.79	78.8
Lobules 4/5	4/5Cb		5.61	78.1
Lobule 6	6Cb		2.50	74.9
Lobule 7	7Cb		0.67	75.2
Lobule 8	8Cb		1.52	75.2
Lobule 9	9Cb		2.81	78.7
Lobule 10	10Cb		1.26	86.7
<i>Lobules of cerebellar hemispheres</i>				
Simple lobule	Sim		4.67	78.4
Crus 1 of the ansiform lobule	Crus 1		4.17	74.6
Crus 2 of the ansiform lobule	Crus 2		4.18	74.6
Paramedian lobule	PM		3.59	76.4
Copula of the pyramis	Cop		2.00	79.7
Paraflocculus	PFl		3.35	72.1
Flocculus	Fl		0.79	79.6
<i>Cerebellar, vestibular, and cochlear nuclei</i>				
Lateral cerebellar nucleus	Lat		0.35	65.2
Lateral cerebellar nucleus, parvicellular part	LatPC		0.05	68.9
Medial cerebellar nucleus	Med		0.28	57.4
Medial cerebellar nucleus, lateral part	MedL		0.02	62.5
Medial cerebellar nucleus, dorsolateral protuberance	MedDL		0.11	60.6
Interposed cerebellar nucleus, anterior	IntA		0.32	60.9
Interposed cerebellar nucleus, posterior	IntP		0.22	62.8
Interposed cerebellar nucleus, posterior parvicellular part	IntPPC		0.04	71.8
Interposed cerebellar nucleus, dorsolateral hump	IntDL		0.10	61.7
Dorsal cochlear nuclei	DC		0.54	77.5
Ventral cochlear nuclei, anterior part	VCA		0.18	70.0
Ventral cochlear nuclei, posterior part	VCP		0.44	66.9
<i>Cerebellar white matter</i>				
Superior cerebellar peduncle	scp		0.25	55.2
Decussation of the superior cerebellar peduncle	xscp		0.09	62.4
Middle cerebellar peduncle	mcp		1.52	47.2
Inferior cerebellar peduncle	icp		0.28	46.7
<i>Other structures</i>				
Dorsal acoustic stria	das		0.03	43.0
Superior medullary velum	SMV		0.04	86.8
Ventral spinocerebellar tract	vsc		0.01	49.3

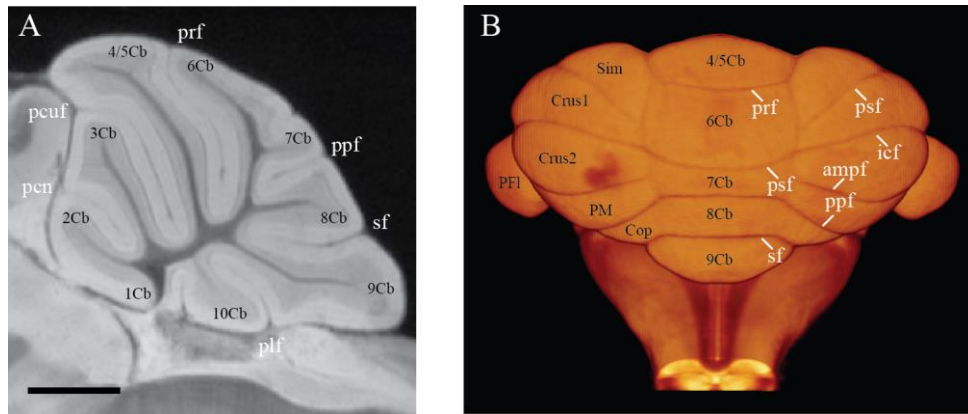


Fig. 1 The lobules and folial pattern of the C57BL/6J cerebellum. (A) Midsagittal section of the cerebellum, scale bar = 1 mm. (B) Surface renderings of the cerebellum. Cerebellar regions are in black and fissures and sulci are in white. Cerebellar regions include: 1Cb, lobule 1 of the cerebellar vermis; 2Cb, lobule 2 of the cerebellar vermis; 3Cb, lobule 3 of the cerebellar vermis; 4/5Cb, lobules 4 and 5 of the cerebellar vermis; 6Cb, lobule 6 of the cerebellar vermis; 7Cb, lobule 7 of the cerebellar vermis; 8Cb, lobule 8 of the cerebellar vermis; 9Cb, lobule 9 of the cerebellar vermis; Cop, copula of the pyramis; Crus 1, crus 1 of the ansiform lobule; Crus 2, crus 2 of the ansiform lobule; PFI, paraflocculus; PM, paramedian lobule; Sim, simple lobule. Fissures include: ampf, ansoparamedian fissure; icf, intercrural fissure; pcn, precentral fissure; pcun, preculminate fissure; plf, posterolateral fissure; ppf, prepyramidal fissure; sf, secondary fissure.

R
↑
↓
C

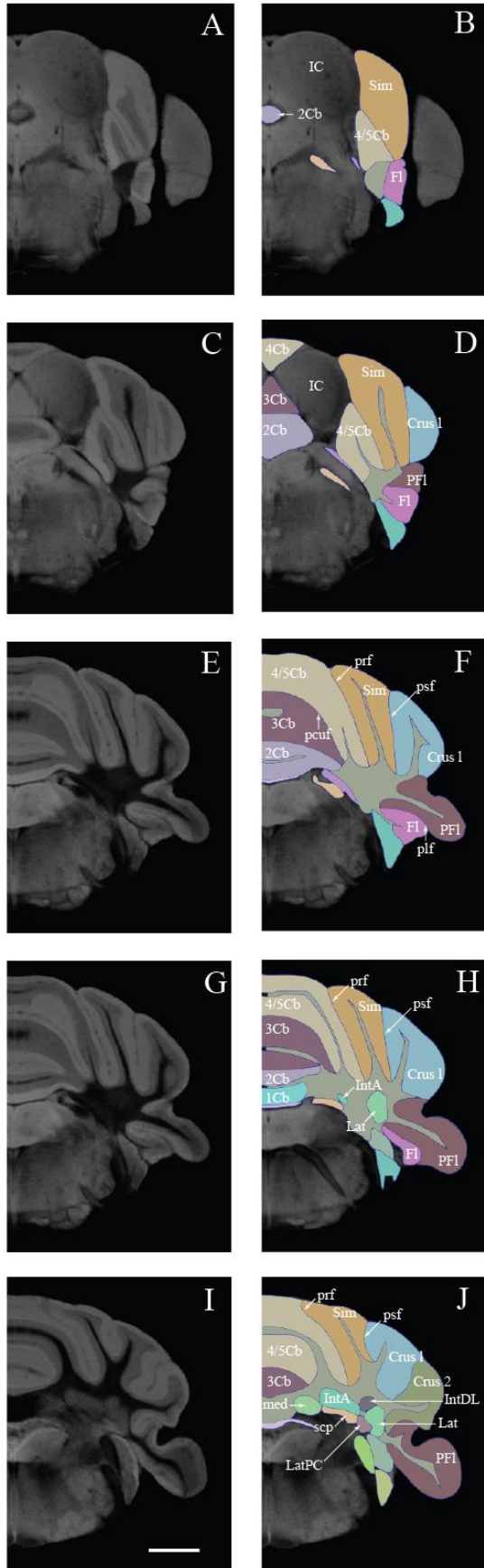


Fig. 2 Segmentation of the rostral vermis and rostral hemispheres. Representative T2* average images (A, C, E, G, I,) and corresponding segmented images (B, D, F, H, I). R-C denotes rostral-caudal direction. Rostral vermis regions include: 1Cb, lobule 1 of the cerebellar vermis; 2Cb, lobule 2 of the cerebellar vermis; 3Cb, lobule 3 of the cerebellar vermis; 4/5Cb, lobules 4 and 5 of the cerebellar vermis. Rostral hemisphere regions include: Crus 1, crus 1 of the ansiform lobule; Crus 2, crus 2 of the ansiform lobule; Fl, flocculus; PFl, paraflocculus; Sim, simple lobule. Cerebellar and vestibular nuclei include: IntA, anterior interpositus nucleus; Lat, lateral cerebellar nucleus; Med, medial cerebellar nucleus; MedDL, medial cerebellar nucleus, dorsolateral extension. Additional abbreviations: IC, inferior colliculi; plf, posterolateral fissure; prf, primary fissure; psf, posterior superior fissure. The color code for all segmented regions is shown in Table 1. Scale bar = 1 mm.

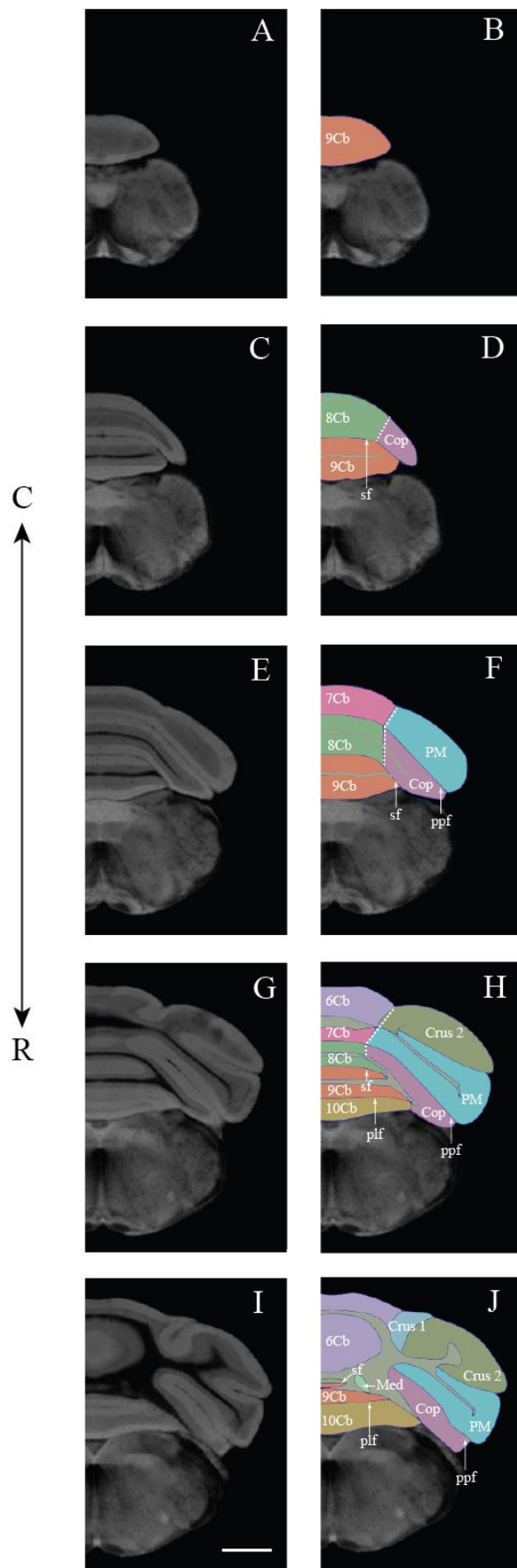


Fig. 3 Segmentation of the caudal vermis and the copula and paramedial lobule. Representative T2* average images (A, C, E, G, I) and corresponding segmented image (B, D, F, H, I). R-C denotes rostral-caudal direction and dashed lines indicate manually delineations required for MRI-based segmentation. Caudal vermal regions include: 10Cb, lobule 10 of the cerebellar vermis; 6Cb, lobule 6 of the cerebellar vermis; 7Cb, lobule 7 of the cerebellar vermis; 8Cb, lobule 8 of the cerebellar vermis; 9Cb, lobule 9 of the cerebellar vermis. Caudal hemisphere regions include: Cop, copula of the pyramis; Crus 1, crus 1 of the ansiform lobule; Crus 2, crus 2 of the ansiform lobule; PM, paramedian lobule. Cerebellar and vestibular nuclei include: Med, medial cerebellar nucleus. Fissures include: plf, posterolateral fissure; ppf, prepyramidal fissure; sf, secondary fissure. The color code for all segmented regions is shown in Table 1. Scale bar = 1 mm.

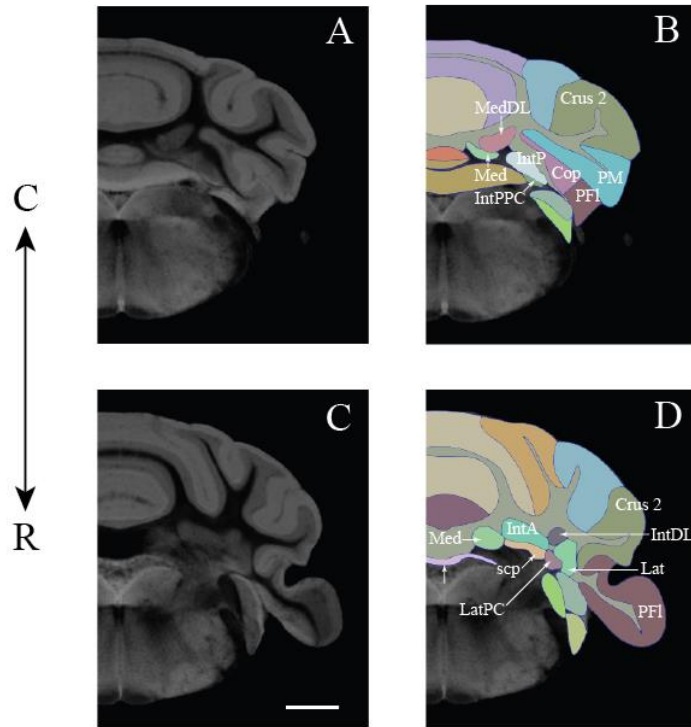


Fig. 4 Segmentation of the central region of the cerebellum. Coronal views of T2* average image (A, C) and corresponding segmented image (B, D). R-C denotes rostral-caudal direction. Hemisphere regions: Cop, copula of the pyramis; Crus 2, crus 2 of the ansiform lobule; PFI, paraflocculus; PM, paramedian lobule. Cerebellar and vestibular nuclei: IntA, interposed cerebellar nucleus, anterior part; IntDL, interposed cerebellar nucleus, lateral part; IntDM, interposed cerebellar nucleus, medial part; IntP, interposed cerebellar nucleus, posterior part; IntPPC, interposed cerebellar nucleus, parvicellular part. Cerebellar white matter: scp, superior cerebellar peduncle. The color code for all segmented regions is shown in Table 1. Scale bar = 1 mm.

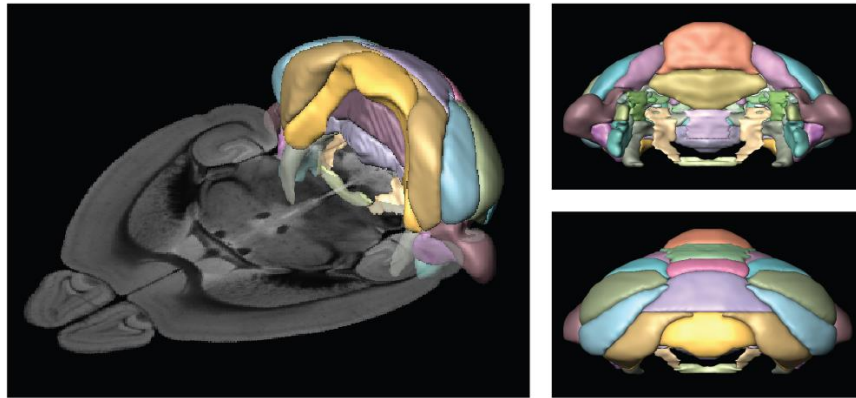


Fig. 5. Colored surface renderings of the segmented vermal and hemispheric lobules and associated structures of the C57BL/6J mouse of the cerebellum in magnetic resonance images. The color code for all segmented regions is shown in Table 1.

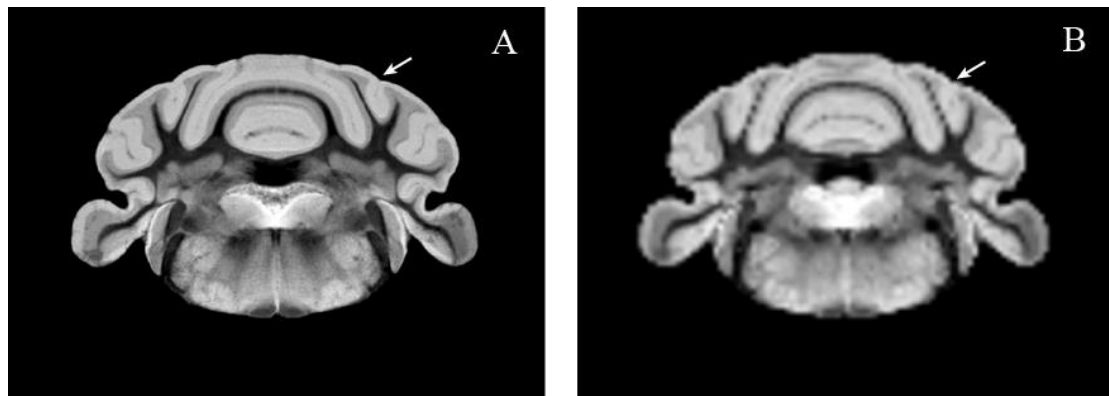
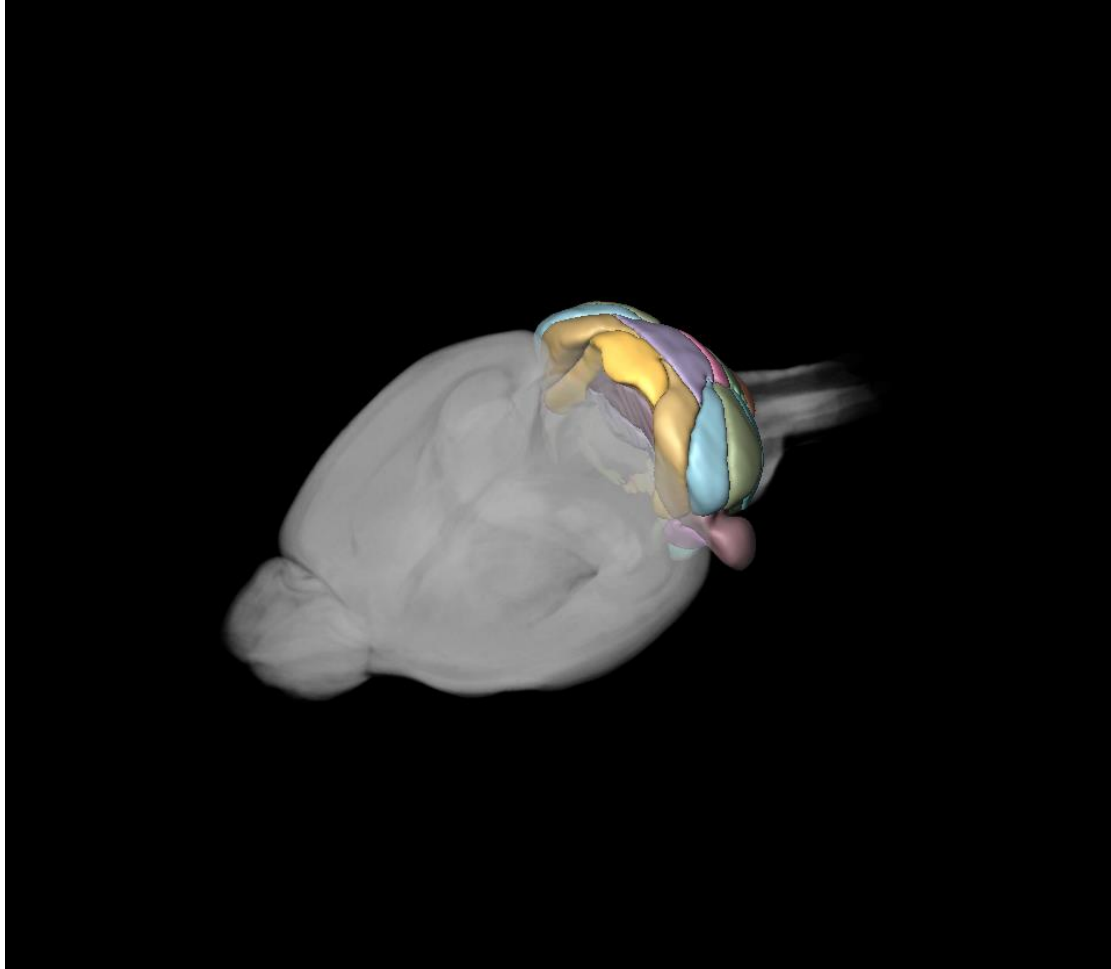


Fig. 6. Comparison of brain region identification between the $15 \mu\text{m}^3$ model (A) and the model downsampled to $100 \mu\text{m}^3$ (B). Noise was not added during downsampling and therefore the signal to noise ratio is artificially higher than true acquired data would be. Note the difficulty in delineating a border between crus 1 of the ansiform lobule and the simple lobule.

Potential Cover Image Volume rendering of C57BL/6J mouse brain with surface rendering of the segmented cerebellum.



References

- Bolk, L., 1906. *Das Cerebellum der Säugetiere*. Jena G. Fischer.
- Collins, D.L., Holmes, C.J., Peters, T.M., Evans, A.C., 1995. Automatic 3-D model-based neuroanatomical segmentation. *Human Brain Mapping* 3, 190-208.
- Donaghy, M., 2009. *Brain's Diseases of the Nervous System*. Oxford University Press, New York.
- Dong, H.W., 2008. *The Allen Reference Atlas: A Digital Color Brain Atlas of the C57Bl/6J Male Mouse*. Hoboken, NJ, US: John Wiley & Sons Inc.
- Dorr, A.E., Lerch, J.P., Spring, S., Kabani, N., Henkelman, R.M., 2008. High resolution three-dimensional brain atlas using an average magnetic resonance image of 40 adult C57Bl/6J mice. *NeuroImage* 42, 60-69.
- Fonov, V., Evans, A.C., Botteron, K., Almli, C.R., McKinstry, R.C., Collins, D.L., 2011. Unbiased average age-appropriate atlases for pediatric studies. *NeuroImage* 54, 313-327.
- Franklin, K., Paxinos, G., 2008. *The mouse brain in stereotaxic coordinates*, 3 ed. Academic Press, San Diego.
- Glickstein, M., 2007. What does the cerebellum really do? *Current Biology* 17, R824-R827.
- Hof, P.R., Young, W.G., Bloom, F.E., Belichenko, P.V., Celio, M.R., 2000. *Comparative Cytoarchitectonic Atlas of the C57BL/6 and 129/Sv Mouse Brains*. Elsevier Academic Press, Amsterdam.
- Inouye, M., Oda, S.I., 1980. Strain-specific variations in the folial pattern of the mouse cerebellum. *The Journal of Comparative Neurology* 190, 357-362.
- Johnson, G.A., Badea, A., Brandenburg, J., Cofer, G., Fubara, B., Liu, S., Nissanov, J., 2010. Waxholm Space: An image-based reference for coordinating mouse brain research. *NeuroImage* 53, 365-372.
- Kovacevic, N., Henderson, J.T., Chan, E., Lifshitz, N., Bishop, J., Evans, A.C., Henkelman, R.M., Chen, X.J., 2005. A three-dimensional MRI atlas of the mouse brain with estimates of the average and variability. *Cereb. Cortex* 15, 639-645.
- Larsell, O., 1952. The morphogenesis and adult pattern of the lobules and fissures of the cerebellum of the white rat. *The Journal of Comparative Neurology* 97, 281-356.
- Larsell, O., 1970. *The Comparative Anatomy and Histology of the Cerebellum from Monotremes Through Apes*. University of Minnesota Press, Minneapolis, MN.
- Ma, Y., Hof, P.R., Grant, S.C., Blackband, S.J., Bennett, R., Slatest, L., McGuigan, M.D., Benveniste, H., 2005. A three-dimensional digital atlas database of the adult C57BL/6J mouse brain by magnetic resonance microscopy. *Neuroscience* 135, 1203-1215.
- Ma, Y., Smith, D., Hof, P., R., Foerster, B., Hamilton, S., Blackband, S.J., Yu, M., Benveniste, H., 2008. *In vivo* 3D digital atlas database of the adult C57BL/6J mouse brain by magnetic resonance microscopy. *Frontiers in Neuroscience* 2, 1-10.
- Neumann, P.E., Garretson, J.D., Skabardonis, G.P., Mueller, G.G., 1993. Genetic analysis of cerebellar folial pattern in crosses of C57BL/6J and DBA/2J inbred mice. *Brain Research* 619, 81-88.
- Neumann, P.E., Mueller, G.G., Sidman, R.L., 1990. Identification and mapping of a mouse gene influencing cerebellar folial pattern. *Brain Research* 524, 85-89.

- Quallo, M.M., Price, C.J., Ueno, K., Asamizuya, T., Cheng, K., Lemon, R.N., Iriki, A., 2010. Creating a population-averaged standard brain template for Japanese macaques (*M. fuscata*). *NeuroImage* 52, 1328-1333.
- Sidman, R.L., Angeviné, J.B., Pierce, E.T., 1971. *Atlas of the mouse brain and spinal cord*. Harvard University Press, Cambridge, MA.
- Sillitoe, R.V., Fu, Y., Watson, C., 2012. Cerebellum. In: Watson, C., Paxinos, G., Puelles, L. (Eds.), *The Mouse Nervous System*. Elsevier Academic Press, San Diego, pp. 361-397.
- Watson, C., Paxinos, G., 2010. *Chemoarchitectonic Atlas of the Mouse Brain*. Elsevier Academic Press, San Diego.

Supplemental Data

Segmentation of the rostral vermis and rostral hemisphere in a rostrocaudal series of coronal images

The most rostral parts of the cerebellum first appear lateral to the two inferior colliculi (IC) and then between the colliculi. Lateral to each colliculus is the lateral extension of the combined lobule 4/5 (4/5Cb), and just below is the flocculus (Fl) (Fig. 2A, B). Between the two colliculi the first part of the vermis to appear is lobule 2 (2Cb), closely followed by lobule 3 (3Cb). Both of these are nested in the space between colliculi. The central (vermal) part of lobule 4/5 (4/5Cb) appears dorsal to the colliculi (Fig. 2C, D). At this level the lateral extension of 4/5Cb is joined dorsolaterally by the simple lobule (Sim) and the rostral part of crus 1 of the ansiform lobule (Crus 1). At the level of disappearance of the inferior colliculi (Fig. 2E, F), the vermis can be clearly seen to consist of 2Cb, 3Cb, and 4/5Cb in order from ventral to dorsal, and it joins with the lateral cerebellar elements (Sim, Fl, Crus 1, PFl, and Fl) and the anterior part of the ventral cochlear nuclei (VCA). This pattern is maintained until (Fig. 2G, H) lobule 1 of the vermis (1Cb) can be identified, and the Fl begins to disappear. At this level, Crus 1 of the hemisphere is joined by crus 2 of the ansiform lobule (Crus 2), as well as the first of the cerebellar nuclei, the lateral cerebellar nucleus (Lat) and the anterior interposed nucleus (IntA) are visible, and the dorsal cochlear nuclei (DC).

Caudal to this (Fig. 2I, J), the vermal part of 4/5Cb starts to disappear as it is covered dorsally by the medial extensions of lobule 6 (6Cb). Note that the simple lobule does not belong to the anterior lobe, because it is a rostral projection of the lateral part of 6Cb. The fissure that separates 4/5Cb from Sim and 4/5Cb from 6Cb is the primary fissure (prf). Following this fissure is crucial to the identification of the caudal part of 4/5Cb, which later becomes submerged under the expanding 6Cb. At this level all of the groups of cerebellar nuclei can be seen in the deep cerebellar white matter, the lateral cerebellar nucleus (Lat), the anterior interpositus cerebellar nucleus (IntA), and the medial cerebellar nucleus (Med) (which later develops a prominent dorsolateral extension, MedDL). In addition, the anterior part of the ventral cochlear nuclei has been replaced by the posterior part, (VCP) and caudal to the cerebellar and cochlear nuclei, lobule 1 is replaced by the rostral tip of lobule 10.

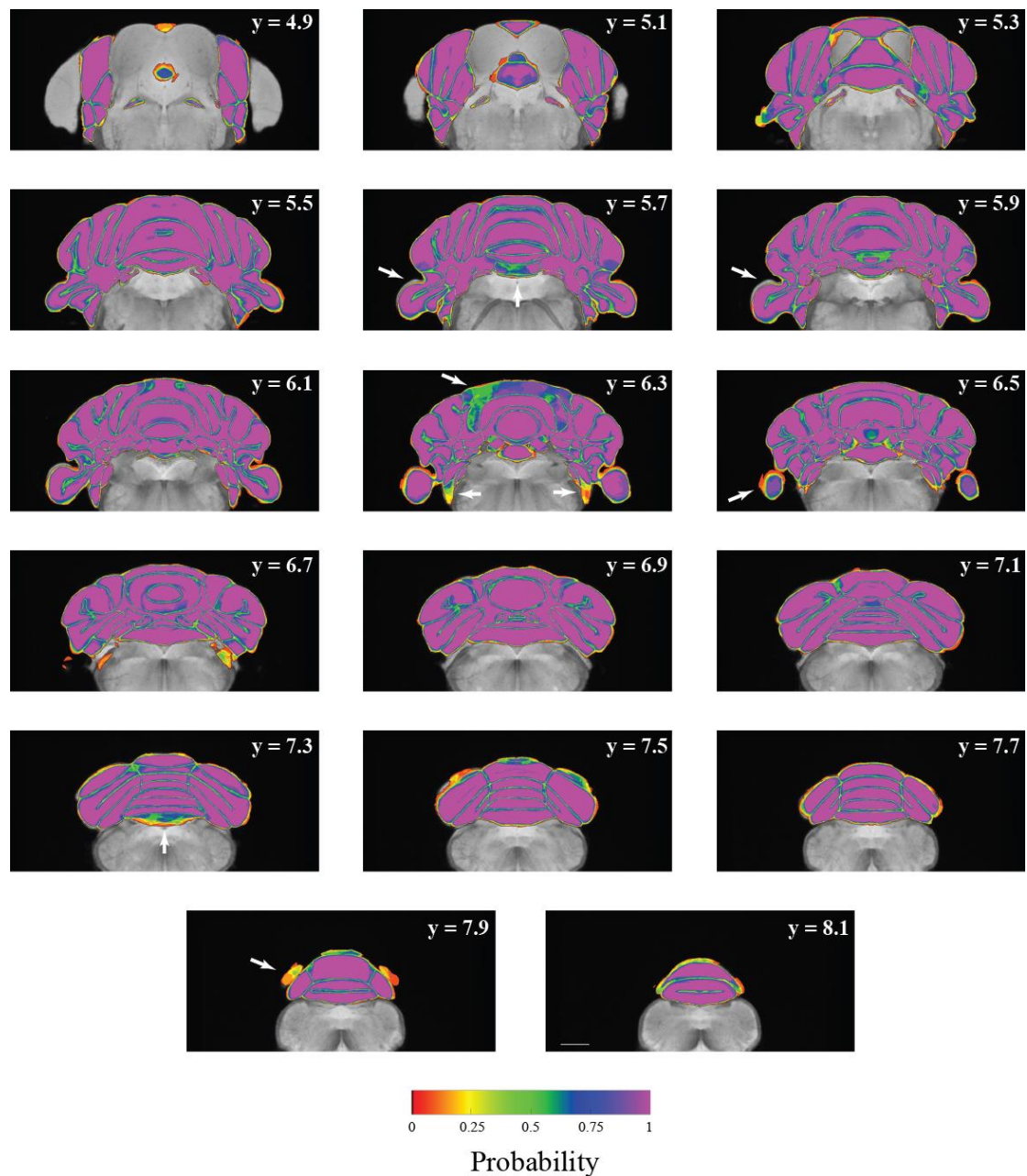
Segmentation of the caudal vermis and the copula and paramedial lobule in a caudorostral series of coronal images

For demarcation of the caudal cerebellum into lobules we advise examining coronal MR images in a caudal to rostral series. At the caudal tip of the vermis is lobule 9 (9Cb) (Fig. 3A, B). Next to appear, dorsal to 9Cb, is lobule 8 (8Cb) (Fig. 3C, D), which is separated from 9Cb by the secondary fissure (sf). The lateral extension of 8Cb is the copula (Cop). The identification of the line of separation of the vermal region from the hemisphere in the mouse is often difficult. In the rat, the paramedian sulcus is usually distinct at the lateral edge of caudal lobule 6, and can be used as the boundary between vermis and hemisphere, but in the mouse it is often difficult to identify. Therefore we delineated the border between the vermal and hemisphere components by first drawing a horizontal straight line through the long axis of the white matter layer in the core of the lobule coronal section. A second line was then drawn through the white matter along the long axis of the hemisphere component.

The point where these two lines intersect was taken as a marker for the lateral margin of the vermis (dotted line Fig. 3F, H). More rostrally lobule 7 (7Cb) appears dorsal to 8Cb, and is separated from 8Cb by the prepyramidal fissure (ppf). 7Cb develops a large lateral extension, called the paramedian lobule (PM) (Fig. 3E, F, which is joined dorsally by Crus 2. 6Cb of the vermis, appears dorsal to 7Cb (Fig. 3G, H). At this level, 10Cb appears ventral to 9Cb, but the line of division is difficult to define. More rostrally the two lobules become distinct (Fig. 3I, J), and are separated by the posterolateral fissure (plf) - the same fissure that separates the flocculus from the paraflocculus (See Fig. 1).

Segmentation of the central region of the cerebellum in a caudorostral series of coronal images

Advancing further rostrally, the copula begins to disappear and is replaced in that position by the caudal end of the paraflocculus (Fig. 4A, B). At this level the posterior interposed cerebellar nucleus (IntP) separates the medial interposed cerebellar nucleus (IntDM) from the lateral interposed cerebellar nucleus (IntDL). The posterior interposed nucleus is bordered ventrally by a distinct parvicellular part (IntPPC). More rostrally (Fig. 4C, D), PM becomes smaller and is absorbed into Crus 2, and paraflocculus becomes very large. At this level there is a major change in the cerebellar nuclei, as the posterior interposed nucleus is replaced by the anterior interposed cerebellar nucleus (IntA). The best indicator of this change is the appearance of the dark band of fibers forming the superior cerebellar peduncle (scp) ventral to the anterior interposed nucleus.



Supplemental Fig. 1. Probabilistic volumes for the C57BL/6J cerebellum. A probability of 1 (100%) means that all individual segmentations on 18 brains overlap on a given voxel. Some areas with the greatest variability are indicated with arrows. Slice positions are given in Waxholm space. Scale bar = 1 mm.

Supplementary Video 1 Colored surface rendering of the segmented cerebellar and associated structures. The color code for all segmented regions is shown in Table 1.

Supplementary Video 1 Surface rendering of the whole mouse brain followed by a horizontal slice series and a colored surface rendering of the segmented cerebellar and associated structures. The color code for all segmented regions is shown in Table 1.